Vibronic Coupling between Soret and Higher Energy Excited States in Iron(II) Porphyrins: Raman Excitation Profiles of A_{2g} Modes in the Soret Region

Tsuyoshi Egawa,*,† Noriyuki Suzuki,‡ Takashi Dokoh,‡ Tsunehiko Higuchi,‡,§ Hideo Shimada,† Teizo Kitagawa,|| and Yuzuru Ishimura†,⊥

Department of Biochemistry, School of Medicine, Keio University, Shinjuku-ku, Tokyo 160-8582, Graduate School of Pharmaceutical Sciences, The University of Tokyo, Hongo, Bunkyo-ku, Tokyo 113-8654, and Institute for Molecular Science, Okazaki National Research Institutes, Myodaiji, Okazaki 444-8585, Japan

Received: June 4, 2003; In Final Form: October 1, 2003

Resonance Raman spectra were observed for heme proteins and iron(II) porphyrins including ferrous−CO and ferrous−isocyanide derivatives of cytochrome $P450_{cam}$, a synthetic iron(II) porphyrin complex having a thiolate axial ligand, ferrous−isocyanide derivative of myoglobin, and synthetic iron(II) porphyrin complexes having either an imidazole or a sulfide axial ligand. Among them, the former three were found to be a hyperporphyrin, giving red and blue Soret absorption bands, whereas others were normal porphyrins giving a single Soret band. When Raman scattering was excited within the Soret region, an anomalously polarized (ap) Raman line, which was assignable to the ν_{19} mode belonging to the A_{2g} species, was observed at 1537−86 cm^{-1} for all these compounds. Both the synthetic iron(II) porphyrins having the imidazole and sulfide ligands also showed another ap Raman line at 1230 cm^{-1}, which was assigned to ν_{26} of A_{2g} symmetry. Raman excitation profiles of the ν_{19} and ν_{26} modes showed a maximum that was displaced from the 0−0 component of the Soret or red Soret band toward higher frequencies by the frequency of the corresponding mode, indicating the 0−1 component. Although Raman lines of these modes were also observed upon excitation at the 0−0 component, they were significantly more intense at the 0−1 component. These results, together with nonadiabatic theories about vibronic contribution to Raman intensity, indicated the presence of vibronic coupling between the Soret (or red Soret) excited state and some other electronic excited state(s) located in the blue of the Soret band. The present study hence demonstrates that lower occupied orbitals other than those described in the ordinary four-orbital model and its extended form, which is applicable to the hyperporphyrins, contribute to the Soret (or red Soret) excited states.

Introduction

The optical spectrum of porphyrin has long been the subject of many studies for not only testing theoretical models of configuration interaction or vibronic coupling in molecules with D_{4h} symmetry but also understanding electronic structures of the active sites of heme proteins and related compounds that bear biological importance.[1−5] Free-base porphyrins and most of metalloporphyrins exhibit an intense absorption band at 380−420 nm, ordinarily called Soret band, and a pair of weaker bands around 500−600 nm termed α and β bands in order of increasing energy.[1] Such features of the optical spectrum of porphyrin have been explained by Gouterman's four-orbital model,[1] which involves two accidentally degenerated HOMOs (a_{1u} and a_{2u}) and two degenerated LUMOs (e_{gx} and e_{gy}). Electronic promotions from the HOMOs to LUMOs undergo configuration interactions to produce the allowed Soret (or B^{00}) band and the nearly forbidden α (or Q^{00}) band. Owing to vibronic coupling between the B^{00} and Q^{00} electronic states, some of the absorption intensity is borrowed from the B^{00} into the Q^{00} transition. The vibronic coupling also produces a vibronic sideband (Q^{01}) of Q^{00}, i.e., the β band.

The above picture about the origins of the α and β bands with respect to vibronic coupling has been examined by the technique of Raman excitation profiles (REPs), i.e., plots of Raman intensity versus Raman excitation energy, which is one of the most powerful tools for investigating electronic excited states of molecules.[6−11] It has been observed that Raman lines of porphyrin skeletal vibration with B_{1g}, B_{2g}, and A_{2g} symmetry, which effectively mix the B^{00} and Q^{00} electronic states and hence gain Raman intensity by the vibronic mechanism, dominate in resonance Raman (RR) spectra of porphyrins when Raman scattering is excited near the α as well as at the β band.[6−11] REPs of these modes exhibit a maximum that is displaced from the α toward the β band by the frequency of corresponding vibration, demonstrating the nature of the β band as a superimposition of vibronic sidebands.[6,8]

Among vibrational modes described above, the B_{1g} and B_{2g} modes, which give rise to depolarized (dp) Raman lines, can also gain Raman intensity by the Franck−Condon mechanism.[9−12] Although B_{1g} and B_{2g} species in the ideal D_{4h} point group cannot produce nonzero values of the Franck−Condon term, dynamic Jahn−Teller distortions upon electronic excitations make the Franck−Condon term nonzero for the B_{1g} and B_{2g} modes, which are Jahn−Teller active.[9−12] On the other hand, the A_{2g} modes

* To whom correspondence should be addressed. Present address: Department of Physiology and Biophysics, Albert Einstein College of Medicine of Yeshiva University, Jack and Pearl Resnick Campus, 1300 Morris Park Avenue, Bronx, NY 10461. Tel: 718-430-4224. Fax: 718-430-4230. E-mail: tegawa@aecom.yu.edu.

† Keio University.

‡ The University of Tokyo.

§ Present address: Faculty of Pharmaceutical Sciences, Nagoya City University, Tanabe-dori, Mizuho-ku, Nagoya 467-8603, Japan.

|| Institute for Molecular Science.

⊥ Present address: Department of Biochemistry, The University of Texas Health Science Center at San Antonio, San Antonio, TX 78229-3900.

10.1021/jp0355612 CCC: $27.50
Published on Web 12/25/2003

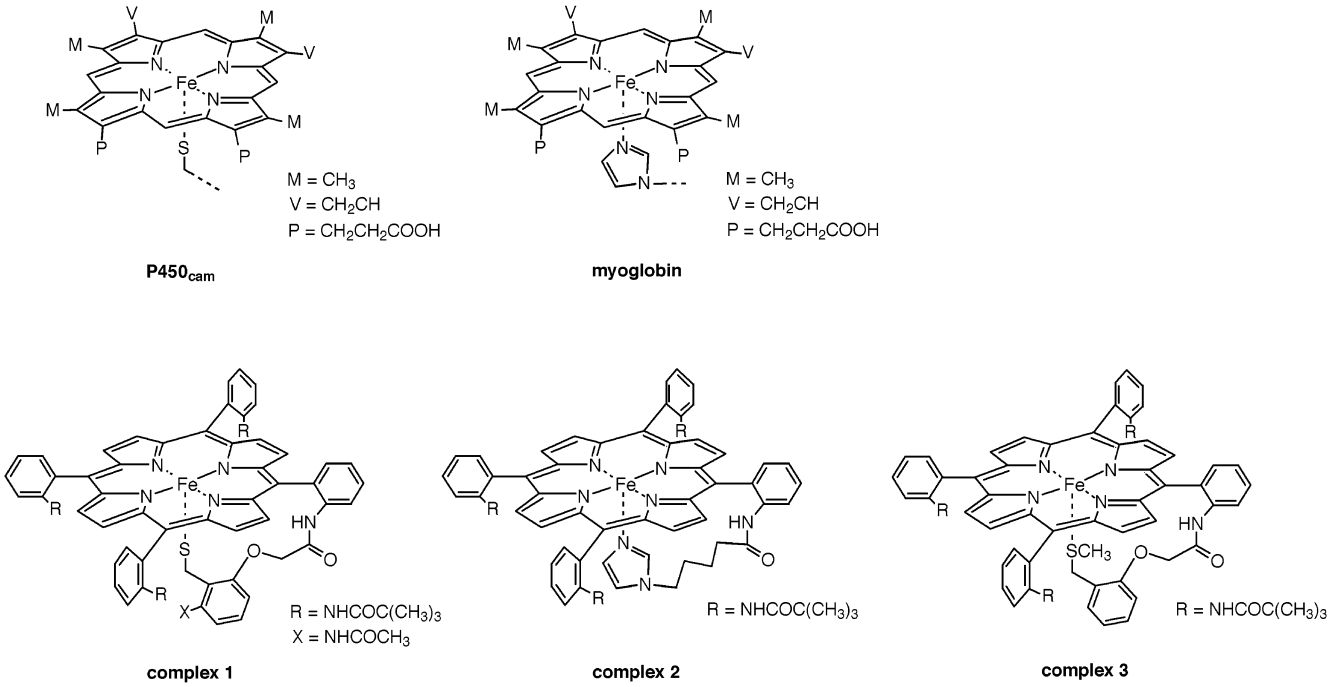

Figure 1. Structures of the active sites of cytochrome $P450_{cam}$ and myoglobin and structures of complexes **1**−**3**.

of porphyrins, which give rise to anomalously polarized (ap) Raman lines, are Jahn−Teller inactive.[10−13] Therefore, for the A_{2g} modes, vibronic coupling between different electronic states (e.g., B^{00} and Q^{00}) is the sole source of Raman intensity.[10−13] In this context, REPs of A_{2g} modes are considered as the best means for elucidating vibronic characters of absorption bands of porphyrins, not being interfered by Franck−Condon contributions to Raman intensity. In contrast to the situation in the studies on the α and β bands, however, REP of A_{2g} mode within the Soret region was not obtained for porphyrins, although observations about A_{2g} Raman lines upon Soret excitation were sometimes reported.[12,14,15]

Here we investigated RR spectra of iron(II) porphyrins including ferrous derivatives of heme proteins and synthetic iron(II) porphyrin complexes using CW lasers of which the frequencies of the incident light beams were tuned to the Soret band. Band-fitting methods and applications of synthetic porphyrins having heavy substituents at the meso positions, in which frequencies of A_{2g} modes were largely shifted from those of other modes, enabled us to obtain REPs of the A_{2g} modes satisfactorily.

Experimental Procedures

Heme Proteins. Ferric form of cytochrome $P450_{cam}$ ($P450_{cam}$) was expressed in *Escherichia coli* strain JM109 and purified according to methods described elsewhere.[16] Sperm whale metmyoglobin was purchased from Sigma and was also purified as already described.[17] The ferrous−CO derivative of $P450_{cam}$ was prepared by reducing ferric $P450_{cam}$ in a CO atmosphere by sodium dithionite. For the preparations of ferrous−isocyanide derivatives of $P450_{cam}$ and myoglobin, ferric $P450_{cam}$ or metmyoglobin was reduced by sodium dithionite in N_2 atmosphere. After the reduction was completed, a water solution of *n*-butylisocyanide (Aldrich) or *tert*-butylisocyanide (id) was introduced anaerobically.

Synthetic Iron Porphyrins. Methods for preparing the synthetic iron(III) porphyrins were previously described.[18−21] These porphyrin complexes have a thiolate (complex 1), imidazole (complex 2), or sulfide (complex 3) as an axial ligand. Their structures are illustrated in Figure 1 together with those of the active sites of $P450_{cam}$ and myoglobin. Iron(II) derivatives of the complexes were prepared by adding a small amount of sodium tetrahydroborate to dimethyl sulfoxide (DMSO) solutions of the complexes in N_2 atmosphere.

RR Spectra. All measurements of RR spectra were carried out at room temperature by using a spinning cell system (1800 rpm). Excitation wavelengths for Raman scattering and corresponding light sources were 406.7 and 441.3 nm, a Kr^+ laser (Spectra Physics, model 2016); 421.0 (±0.5) nm, a diode laser (Hitachi Metals, model ICD-430); 430 (±0.5) nm, another diode laser (id); 441.6 nm, a He−Cd laser (Kinmon Electric, model CD4805R); and 514.5 nm, an Ar^+ laser (NEC, model GLG3200). Scattered light was detected by a liquid N_2-cooled charge-coupled device (CCD) (PAR EG&G, CCD-1340/400-EB) attached to a single polychromator (Ritsu Oyo Kogaku, DG-1000).

The incident light beam for Raman excitation was introduced vertically into the spinning cell from the bottom side of the cell, and the scattered light along 90° from the incident light was collected. The polarization of the incident light was held perpendicular to the scattering direction. The scattered light was passed through a polarizer. Between the polarizer and the polychromator was placed a polarization scrambler. The instrument function of the present spectrophotometric system with respect to the sensitivity to photon depended on the geometry (parallel versus perpendicular to the polarization of the incident light) of the polarizer. This dependency was compensated on the basis of spectra of white light, which were recorded under the parallel and perpendicular geometries.

Band Fitting Analyses. Calculations of band fits were carried out by using Igor software (Wave Metrics Inc.) on a Macintosh computer.

Results

Resonance Enhancement of ν_{19} of Hyperporphyrins: Ferrous−CO $P450_{cam}$. Figure 2 shows RR spectra of the ferrous−CO derivative of $P450_{cam}$ in parallel (∥) and perpendicular (⊥) polarizations excited at 406.7 or 421.0 nm. In the

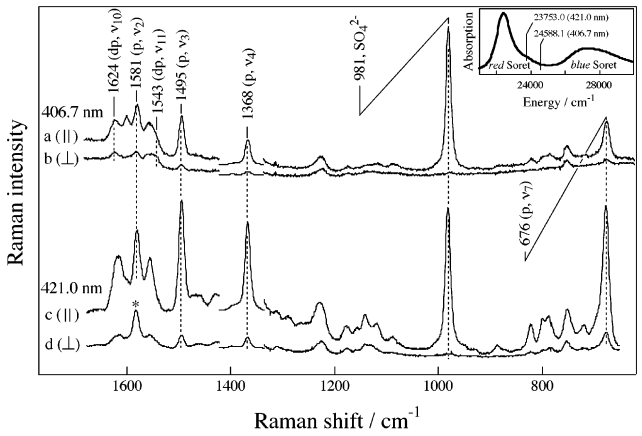

Figure 2. RR spectra of the ferrous−CO derivative of $P450_{cam}$ in parallel (||) and perpendicular (⊥) polarization upon excitation wavelengths at 406.7 and 421.0 nm. $P450_{cam}$ (30 μM) was dissolved in a buffer containing 50 mM potassium phosphate (pH 7.4), 1 mM *d*-camphor, and 5% ammonium sulfate. The inset shows the optical absorption spectrum of ferrous−CO $P450_{cam}$ in the Soret region together with energies of the incident light beams at 406.7 and 421.0 nm.

inset, the Soret absorption spectrum of ferrous−CO $P450_{cam}$ is shown together with the energies of the incident light beams (406.7 and 421.0 nm correspond to 24588.1 and 23753.0 cm^{-1}, respectively). It is well-known that ferrous−CO $P450_{cam}$ is one of the hyperporphyrins [22−24] characterized by their unique Soret bands being split into two components (blue and red Soret bands) owing to the occurrence of configuration interaction between a certain charge transfer (CT) state and the porphyrin B^{00} excited state.[1] For the case of ferrous−CO $P450_{cam}$, a CT transition from the thiolate axial ligand to the heme has been believed to play such a role in the splitting of the Soret band.[22,23] Although other mechanisms were also proposed for the Soret band splitting of $P450_{cam}$, these mechanisms also involve crucial roles of the thiolate ligand in the splitting.[25, 26]

Upon excitation at 406.7 nm, several Raman lines appeared in either parallel (spectrum a) or perpendicular (spectrum b) polarization. Among them, a Raman line at 981 cm^{-1} in parallel polarization arises from SO_4^{2-} of ammonium sulfate (5%), which was contained in the samples as an off-resonance internal standard for Raman intensity. For some other Raman lines, polarization property (p, polarized; dp, depolarized) was marked. On the basis of the frequencies and the polarization properties, these Raman lines could be assigned to porphyrin core modes as marked in the figure (mode number was according to Abe et al.[27]).

When the excitation wavelength was tuned to 421.0 nm, changes in Raman intensity with respect to the internal standard (SO_4^{2-}) were observed for ν_3, ν_4, and ν_7 (spectra c and d) all of which belong to A_{1g} species in the D_{4h} symmetry. However, notable changes in the depolarization ratio, ρ ($\rho = I_\perp/I_{||}$, where $I_\perp$ and $I_{||}$ represent band intensities of Raman line in perpendicular and parallel polarization, respectively), were not found for these modes upon the change of the excitation wavelength.

On the other hand, band features around ν_2 in the 421.0 nm excited spectra seem somewhat strange. In spectrum d, an intense band (marked with asterisk) is found in perpendicular polarization at a frequency close to ν_2. The band is almost one-half as intense as its counterpart in parallel polarization, being unlikely as A_{1g} modes, which generally give ρ values about 0.125.[28] Furthermore, as will be shown in the next figure, the band is found to be upshifted by ca. 2 cm^{-1} from ν_2. Thus, it is most likely that a certain mode, whose frequency is close to

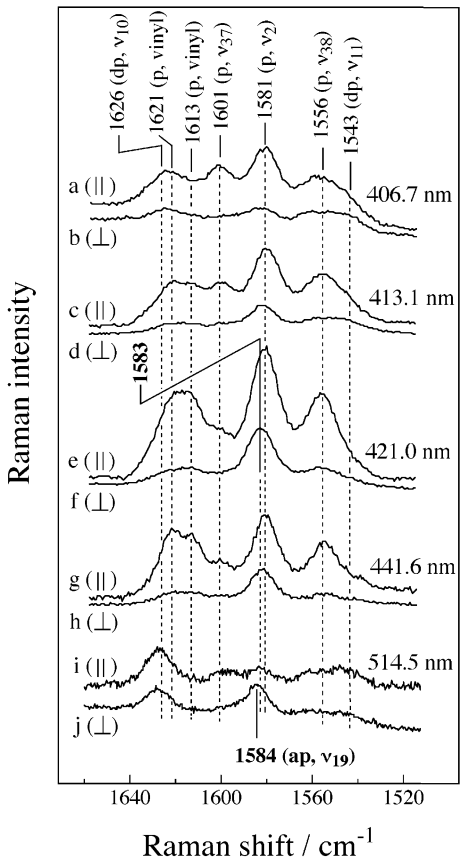

Figure 3. RR spectra of ferrous−CO $P450_{cam}$ in the 1520−1650 cm^{-1} region upon excitation wavelengths within the red Soret (a−h) and Q (i and j) bands. For all the measurements, the buffer system used was the same as that for Figure 2, except that the spectra i and j were measured in absence of ammonium sulfate. The concentration of $P450_{cam}$ was 30 μM for a−h and 100 μM for i and j.

ν_2, gives rise to dp or anomalously polarized (ap) Raman line upon excitation at 421.0 nm. This phenomena is quite similar to that noted for Ni(OEP) excited at 514.5 nm.[29]

Studies of normal coordinate analyses have revealed all porphyrin core modes, which give rise to Raman lines in a frequency range from 1520 to 1650 cm^{-1}. They include ν_2 (A_{1g}), ν_{37} (E_u), ν_{38} (E_u), ν_{10} (B_{1g}), ν_{11} (B_{1g}), and ν_{19} (A_{2g}).[27] Among them, modes which give dp Raman lines are ν_{10} and ν_{11}, whereas the mode giving an ap line is ν_{19}. In the RR spectra of ferrous−CO $P450_{cam}$, ν_{10} and ν_{11} are found at frequencies (1624 and 1543 cm^{-1}, respectively) distinct from ν_2 at 1581 cm^{-1} (spectrum b). Therefore, it is most likely that the ν_{19} mode is the mode in question, which gave rise to a Raman line at around the frequency of ν_2 in perpendicular polarization upon 421.0 nm excitation.

To investigate Raman enhancement pattern of ferrous−CO $P450_{cam}$ in detail, we measured RR spectra using other excitation wavelengths. Spectra thus obtained are illustrated in Figure 3 together with the 406.7 and 421.0 nm excited RR spectra shown in Figure 2. The vertical scales of spectra a−h were normalized by using the SO_4^{2-} band at 981 cm^{-1} described above. Excitation wavelengths for spectra a−h (406.7−441.6 nm) are contained in the red Soret band of ferrous−CO $P450_{cam}$, whereas that for spectra i and j (514.5 nm) coincides with the β (or Q^{01}) band. The 421.0 nm excited RR spectra (e and f) clearly show that the 1583 cm^{-1} band in perpendicular polarization is shifted from the parallel band of ν_2 at 1581 cm^{-1}. Furthermore, the Q band excited spectra (i and j) demonstrate that ν_{19} of ferrous−CO $P450_{cam}$ lies at 1584 cm^{-1}. These findings further support

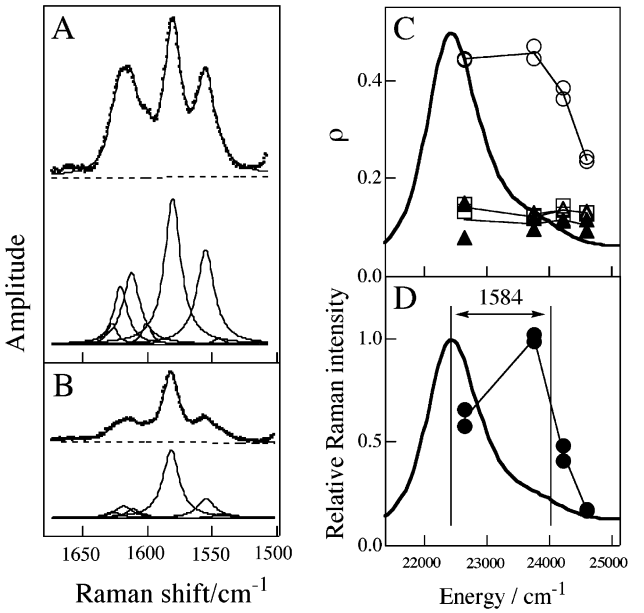

Figure 4. Results of band fitting analyses on the RR spectra of ferrous−CO P450$_{cam}$. (A) and (B) Lorentzian profiles were calculated for the spectra e and f in Figure 3 assuming the presence of seven Lorentzian-type bands. Each bottom of (A) and (B) shows the calculated profiles, whereas each top shows the sum of the profiles (broken line) together with the observed spectrum (solid line). (C) Plots of ρ versus the excitation energy for Raman scattering: open circle, $I_{\perp}^{app}/I_{\parallel}^{app}$ (see text); open triangle, ν_7; closed triangle, ν_3; open square, ν_4. (D) REP of the ν_{19} mode. Data of the relative band intensity of the ν_{19} mode were obtained as described in the text. In (C) and (D), the red Soret band of ferrous−CO P450$_{cam}$ is also illustrated on arbitrary vertical scales.

the assignment of the perpendicular band to ν_{19}. Accordingly, we conclude that ν_{19} of ferrous−CO P450$_{cam}$ gains significant Raman intensity upon excitation within the Soret region, although the intensity eancement of A_{2g} modes had been thought to occur only in the Q band region.

As already described, the porphyrin skeleton gives six Raman lines in the 1520−1650 cm^{-1} region (ν_2, ν_{37}, ν_{38}, ν_{10}, ν_{11}, and ν_{19}). Protoporphyrin IX, which is the chromophore of P450$_{cam}$ and myoglobin, frequently exhibits two more polarized Raman lines attributed to $\nu_{C=C}$ of two vinyl substituents.[30−32] They are found at 1621 and 1613 cm^{-1} in spectrum g. Thus, all the modes of ferrous−CO P450$_{cam}$ gain Raman intensity upon excitation in the Soret region, as shown in Figure 3. Appearance of Raman inactive E_u modes such as ν_{37} (1601 cm^{-1}) and ν_{38} (1556 cm^{-1}) in spectra a and g, respectively, mean that the D_{4h} symmetry is not exactly retained. Upon saddling and doming, which are the two practical deformations of metalloporphyrins, E_u species of D_{4h} are combined with E_g into Raman active E species of D_{2d} (saddling) or of C_{4v} (doming).[33] On the other hand, A_{2g} of D_{4h} are combined with B_{2u} or A_{1u} into A_2 species of D_{2d} and C_{4v}, which are still Raman inactive with respect to the Franck−Condon mechanisms.[33] Therefore, the intensity enhancement of ν_{19} of ferrous−CO P450$_{cam}$ is not due to the lowering of symmetry from D_{4h}.

On the basis of the above assignments, we performed a series of band fitting analyses for spectra a−h in Figure 3. Parts A and B of Figure 4 show results of the analyses carried out for spectra e and f in Figure 3, respectively. The observed RR spectra were well reproduced as a sum of deconvoluted bands. Similar results were also obtained when analyses were done on other spectra in Figure 3 (not shown). Although the possible number of Raman lines is eight (ν_2, ν_{37}, ν_{38}, ν_{10}, ν_{11}, ν_{19}, and $\nu_{C=C}$ of two vinyl groups), we performed the analyses assuming the presence of seven Lorentzian-type bands in each spectrum, because Raman lines of ν_2 and ν_{19}, which are very close in frequency, could not be resolved in the present analyses. Thus each deconvoluted band at 1581−4 cm^{-1} corresponds to the sum of ν_2 and ν_{19} Raman lines. For convenience, band intensities of such deconvoluted bands at 1581−4 cm^{-1} in parallel and perpendicular polarization are denoted by $I_{\parallel}^{app}$ and $I_{\perp}^{app}$, respectively. In Figure 4C, apparent ρ, i.e., $I_{\perp}^{app}/I_{\parallel}^{app}$, is plotted against the energy of the incident light (open circle) together with the optical absorption of the red Soret band of ferrous−CO P450$_{cam}$ (solid line). For comparison, ρ values obtained in this study for Raman lines of A_{1g} modes of ferrous−CO P450$_{cam}$, such as ν_3 (closed triangle), ν_4 (open square), and ν_7 (open triangle), are also plotted in Figure 4C. The ρ values of these A_{1g} modes were essentially unchanged over the excitation energies examined here, being in good agreement with the theoretical value (0.125).[28] Therefore, it can be reasonably assumed that the actual ρ value of ν_2 of ferrous−CO P450$_{cam}$ is also about 0.125, and accordingly, the data in Figure 4C (open circle) indicate that ν_{19} gains Raman intensity upon all excitation wavelengths examined.

Although the present band fitting analyses could not directly reveal band intensity of ν_{19} of ferrous−CO P450$_{cam}$, the parameters $I_{\parallel}^{app}$ and $I_{\perp}^{app}$ are expected to involve contributions form ν_2 and ν_{19}. To obtain the Raman excitation profile (REP) of ν_{19}, we assumed first, $I_{\perp}[\nu_2] = 0.125I_{\parallel}[\nu_2]$, and second that ν_{19} scarcely gives rise to Raman intensity in parallel polarization. The latter assumption appears reasonable as demonstrated by the Q band excited RR spectra (spectra i and j in Figure 3). These two assumptions allow us to deduce the band intensity of ν_{19} ($I[\nu_{19}]$) to be given by $I[\nu_{19}] = I_{\perp}^{app} - 0.125I_{\parallel}^{app}$. In Figure 4D, $I[\nu_{19}]$ thus obtained are plotted against the energy of the incident light together with the optical absorption (solid line) of the red Soret band of ferrous−CO P450$_{cam}$. The plot, REP of ν_{19}, shows a maximum, which is significantly displaced from the absorption maximum at 22422 cm^{-1}. If ν_{19} (1584 cm^{-1}) gives rise to a 0−1 sideband via vibronic coupling, the sideband is expected to appear at 24 006 cm^{-1} (22 422 cm^{-1} + 1584 cm^{-1} = 24 006 cm^{-1}). The maximum position of the REP is in reasonable agreement with that of the possible 0−1 sideband.

It is well-known that in-plane and out-of-plane porphyrin deformations cause dispersion in depolarization ratios and affect shapes of REPs.[34] The deformations affect ρ of the A_{2g} modes most significantly; they frequently decrease the ρ of A_{2g} modes from the typical value (∼30) in planar porphyrins to 2−3.[34] However, as far as we observed RR spectra upon visible excitation, the Raman intensity of the ν_{19} mode was essentially neglidgeble in the parallel polarization (Figure 3, i and j). Therefore, it can be reasonably assumed that contributions of the deformations are also negligible in RR spectra at the Soret excitation.

Resonance Enhancement of ν_{19} of Hyperporphyrins: Isocyanide Derivatives of Ferrous P450$_{cam}$. In the next series of experiments, we measured and analyzed RR spectra of isocyanide derivatives of ferrous P450$_{cam}$ (Figure 5A). The derivatives have also been categorized as hyperporphyrins.[24] In Figure 5B, optical absorption spectrum of *n*-butylisocyanide adduct of ferrous P450$_{cam}$ is shown. When Raman scattering was excited at 421.0 nm, the *n*-butylisocyanide adduct exhibited an ap Raman line at 1584 cm^{-1} (spectra a and b in Figure 5A), which was assignable to the ν_{19} mode. The ν_{19} Raman line was weakened significantly when the excitation wavelength was tuned to 406.7 nm (spectra c and d). Resonance enhancement

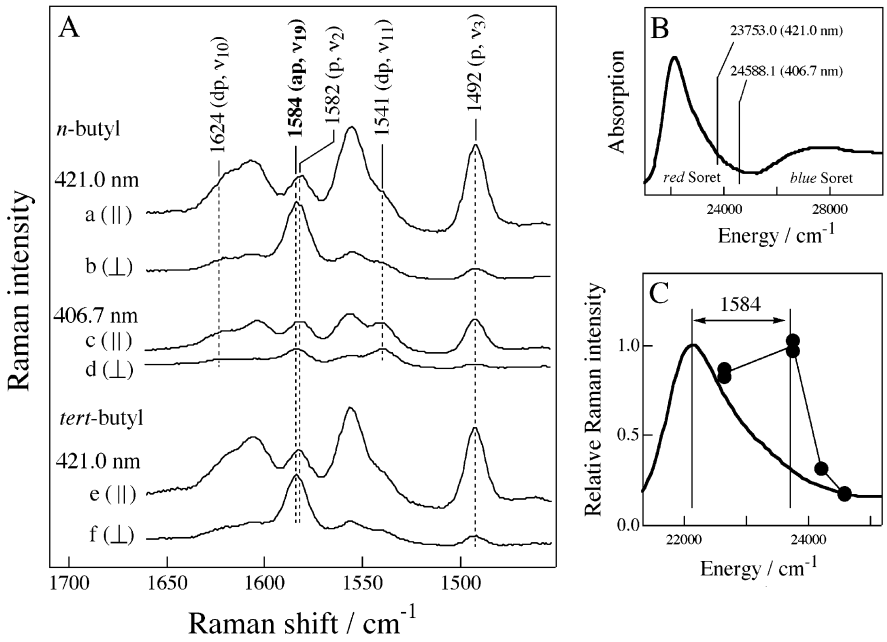

Figure 5. Resonance enhancements of the ν_{19} Raman line of ferrous−isocyanide P450$_{cam}$ derivatives upon excitation within the red Soret band. (A) RR spectra of the ferrous−*n*-butylisocyanide (a−d) and ferrous−*tert*-butylisocyanide (e and f) derivatives of P450cam upon excitation wavelengths at 406.7 and 421.0 nm. P450cam (30 μM) was dissolved in a buffer containing 50 mM potassium phosphate (pH 7.4), 100 μM *d*-camphor, 5% ammonium sulfate, and 32 mM *n*- or *tert*-butylisocyanide. (B) Absorption spectrum of the ferrous−*n*-butylisocyanide derivative of P450cam in the Soret region and energies of the incident light beams at 406.7 and 421.0 nm. (C) REP of the ν_{19} mode of the ferrous−*n*-butylisocyanide derivative of P450cam. In (C), the red Soret band of the ferrous−*n*-butylisocyanide derivative is also illustrated on an arbitrary vertical scale.

of the ν_{19} Raman line upon excitation at 421.0 nm was also found for the *tert*-butylisocyanide adduct (spectra e and f). For the *n*-butylisocyanide adduct, we performed band fitting analyses essentially the same as those employed for the ferrous−CO derivative and obtained a REP of ν_{19} as shown in Figure 5C. Similar to the case of the ferrous−CO derivative, the REP of the *n*-butylisocyanide adduct shows a maximum that is displaced from that of the red Soret band by an energy close to the vibration energy of ν_{19}.

Resonance Enhancement of ν_{19} of Normal Porphyrins: Isocyanide Derivatives of Myoglobin. The unexpected REP behaviors of the ν_{19} Raman lines described above were seen for hyperporphyrins. To examine whether ordinary porphyrins (normal porphyrins) also exhibit Raman lines of ν_{19} or other A_{2g} modes upon Soret excitation, we carried out RR experiments using myoglobin, which employs a histidylimidazole as the axial ligand. Derivatives of myoglobin such as ferrous−CO or ferrous−isocyanide forms are all normal porphyrins.[35] The optical absorption spectrum of *n*-butylisocyanide adduct of myoglobin is shown in Figure 6B. When Raman scattering was excited at 406.7 nm, the *n*-butylisocyanide adduct of myoglobin exhibited an intense Raman line at 1586 cm^{-1} in perpendicular polarization (Figure 6A, spectrum b). The Raman line was comparable in intensity to its counterpart in parallel polarization (spectrum a). The frequency of 1586 cm^{-1} is in complete agreement with the ν_{19} frequency at 1587 cm^{-1}, which was determined on the basis of Q band excited RR spectra (spectra e and f), indicating that ν_{19} of the *n*-butylisocyanide adduct of myoglobin also gained Raman intensity upon Soret excitation. The ν_{19} Raman line almost disappeared when the excitation wavelength was tuned to 421.0 nm (spectra c and d). All these observations were reproducible in the *tert*-butylisocyanide adduct of myoglobin (not shown). Accordingly, it demonstrates that the resonance enhancement of the ν_{19} mode upon excitation within the Soret region takes place not only in hyperporphyrins but also in normal porphyrins.

For RR spectra of the *n*-butylisocyanide adduct of myoglobin, we performed band-fitting analyses essentially in the same way as those described already. Figure 6C shows REP of ν_{19} (circle) thus calculated. The apparent ρ values (see above) were also shown (triangle). Although the maximum position of the REP could not be determined in the range of the excitation energy examined here, it is clear that the ν_{19} Raman line is more intensified at the higher energy side of the Soret maximum. These findings suggest that ν_{19} of the *n*-butylisocyanide adduct of myoglobin also gains Raman intensity upon excitation within corresponding 0−1 vibronic sideband. Because the Soret band of the *n*-butylisocyanide adduct appears at 23 202 cm^{-1}, the 0−1 band is expected at around 24 800 cm^{-1} (23 202 cm^{-1} + 1587 cm^{-1} = 24 789 cm^{-1}; see Figure 6C).

Separation of ν_{19} and ν_2 Raman Lines and Observations of ν_{26} in Meso-Substituted Porphyrins. The resonance enhancements of ap Raman lines were further investigated with synthetic iron porphyrin complexes, which have a thiolate (complex 1), imdazole (complex 2), or sulfide (complex 3) axial ligand (see Figure 1). Hence, these complexes mimic the active site structures of P450 (complex 1) or other heme proteins such as myoglobin (complex 2). In addition, the porphyrin of these complexes has heavy substituents at all meso positions (Figure 1). Such a substitution at meso positions must induce an appreciable downshift in the ν_{19} frequency, but not in ν_2.[27] If so, ν_{19} and ν_2 Raman lines will be resolved.

All the above complexes were readily reduced to corresponding iron(II) derivatives (iron(II) complexes **1**−**3**) in DMSO by sodium tetrahydroborate, and CO and isocyanide adducts of them were prepared successfully. RR measurements of these CO and isocyanide adducts were, however, very difficult, because photodissociation reactions took place significantly under the present experimental conditions. On the other hand, iron(II) complexes **1**−**3** were all stable over measurements of RR spectra. Thus we used them for the present purpose.

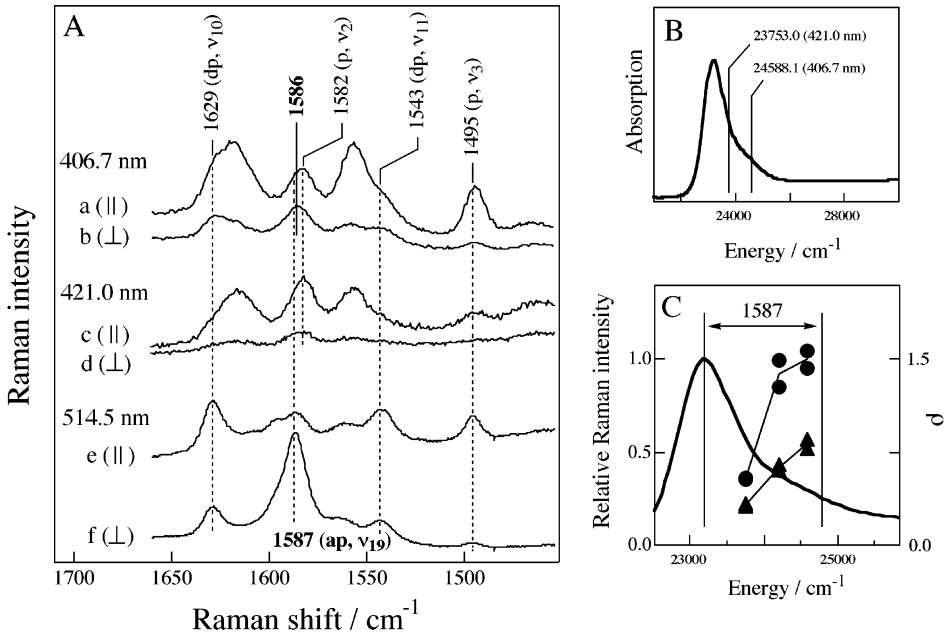

Figure 6. Resonance enhancements of the ν_{19} Raman line of ferrous−*n*-butylisocyanide myoglobin upon excitation within the Soret band. (A) RR spectra of ferrous−*n*-butylisocyanide myoglobin upon excitation wavelengths at 406.7, 421.0, and 514.5 nm. Compositions of the samples were 30 μM myoglobin, 50 mM potassium phosphate (pH 7.4), 32 mM *n*-butylisocyanide, and 5% ammonium sulfate for a−d, and 100 μM myoglobin, 100 mM potassium phosphate (pH 7.3), and 50 mM *n*-butylisocyanide for e and f. (B) Optical absorption spectrum of ferrous−*n*-butylisocyanide myoglobin in the Soret region and energies of the incident light beams at 406.7 and 421.0 nm. (C) REP of ν_{19} (circle) and plot of ρ ($=I_{\perp}^{app}/I_{||}^{app}$) versus the excitation energy for Raman scattering (triangle). The Soret band of ferrous−*n*-butylisocyanide myoglobin is also illustrated on an arbitrary vertical scale.

Iron(II) complex **1**, which has the thiolate axial ligand, exhibited a hyperporphyrin spectrum (λ_{max}; 370 and 448 nm), whereas the iron(II) complex **2** (λ_{max}; 433 nm) and iron(II) complex **3** (λ_{max}; 435 nm) were found to be normal porphyrins. The λ_{max} value of iron(II) complex **2**, which has an imidazole axial ligand, is close to that found for five-coordinate ferrous myoglobin (deoxymyoglobin) at 434 nm.[35] On the other hand, the absorption spectrum of the iron(II) complex 1 is significantly different from that of five-coordinate ferrous $P450_{cam}$, which is known to exhibit a normal porphyrin spectrum (λ_{max}; 411 nm).[36] As already described, the thiolate axial ligand is responsible for the hyperporphyrin spectra of ferrous derivatives of $P450_{cam}$ and also of their models. The thiolate ligand, however, does not necessarily cause the Soret band splitting in the all of the ferrous derivatives of $P450_{cam}$[24,36] as exemplified by the five-coordinate ferrous form, depending on how it donates electrons to the heme in each derivative. Our tentative explanation about the difference between the absorption spectra of iron(II) complex **1** and the five-coordinate ferrous $P450_{cam}$ is that the electron-donating properties of the thiolate ligand are different between them possibly because the difference in the environment around the ligand (protein matrix versus DMSO). This explanation is consistent with the fact that DMSO induces changes in absorption spectra of certain P450 models having a thiolate axial ligand even if it does not ligate to the heme iron of the models.[37]

Figure 7 shows RR spectra of iron(II) complex **1** measured by using excitation wavelengths from 406.7 to 441.6 nm. In the inset, the optical absorption spectrum of this complex, which is of the hyperporphyrin type, is illustrated. The vertical scales of RR spectra were normalized by using a dp Raman line of DMSO at 1419 cm^{-1} (marked with an asterisk), which serves as an off-resonance internal standard for Raman intensity. When Raman scattering was excited at 421.0 nm, the complex exhibited an ap Raman band at 1541 cm^{-1} (spectra e and f), which was assignable to ν_{19}. The frequency of ν_{19} (1541 cm^{-1}) was remarkably lower than that of ν_2 at 1563 cm^{-1}. Owing to the downshift of the ν_{19} frequency, ν_{19} and ν_2 Raman lines are clearly resolved (spectra e and f) as we expected.

The band intensity of the ν_{19} Raman line of iron(II) complex **1** decreased by moving the excitation wavelength from 421.0 nm to shorter wavelengths (Figure 7, spectra a−d). Likewise, it also decreased when the excitation wavelength was moved from 421.0 nm to the longer wavelengths close to the red Soret maximum (spectra g and h), although an appearance of a dp band at 1547 cm^{-1} made it difficult to analyze the intensity changes quantitatively. These observations are quite similar to those found for ferrous−CO and ferrous−isocyanide derivatives of $P450_{cam}$, suggesting that ν_{19} of iron(II) complex **1** gains Raman intensity upon excitation at the corresponding 0−1 vibronic band.

Iron(II) complex **2** also exhibited a well-resolved ν_{19} Raman line at 1537 cm^{-1} upon excitation within the Soret band (Figure 8A, spectra a−d). Besides the ν_{19} Raman line, the complex exhibited another ap Raman line at 1230 cm^{-1}, which is assignable to ν_{26}.[38] The Raman lines of ν_{19} and ν_{26} almost disappeared when excitation wavelength was moved to 430.0 nm (spectra e and f). The ν_{19} Raman line was more intense upon excitation at 406.7 nm as compared to that upon 413.1 nm, whereas the ν_{26} Raman line was found to behave in reverse (spectra a−d). On the basis of the observed RR spectra, REPs of ν_{19} and ν_{26} were obtained as shown in Figure 8B (closed circle, ν_{19}; open circle, ν_{26}; solid curve, Soret absorption of iron(II) complex **2**).

The REP of ν_{26} gives rise to a maximum at the wavelength, which is in an agreement with the sum frequency of the Soret 0−0 transition energy and the vibration energy of ν_{26} (23 095 cm^{-1} + 1230 cm^{-1} = 24 325 cm^{-1}) (411 nm). Similarly, the REP of ν_{19} indicates that its band intensity increases when the excitation energy approaches to the sum of the Soret 0−0 and the ν_{19} vibration energies (23 095 cm^{-1} + 1537 cm^{-1} = 24 632 cm^{-1}) (406 nm). These findings are consistent with the view that ν_{19} and ν_{26} modes take part in vibronic interactions between

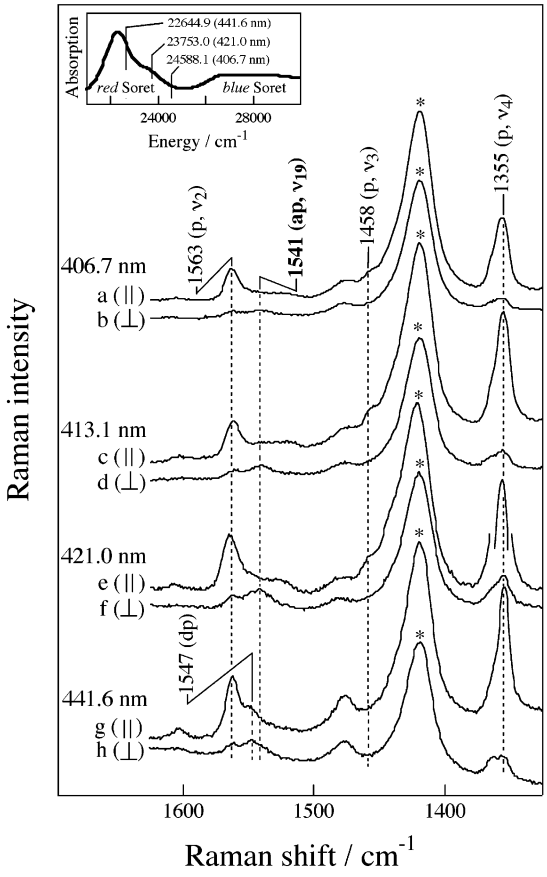

Figure 7. RR spectra of iron(II) complex **1** in DMSO upon excitation wavelengths at 406.7, 413.1, 421.0, and 441.6 nm. The concentration of the sample was 33 μM. The inset shows the optical absorption spectrum of iron(II) complex **1** in the Soret region together with energies of incident light beams at 406.7, 421.0, and 441.6 nm. The position of the energy of the incident light beam at 430 nm is not indicated for clarity of presentation.

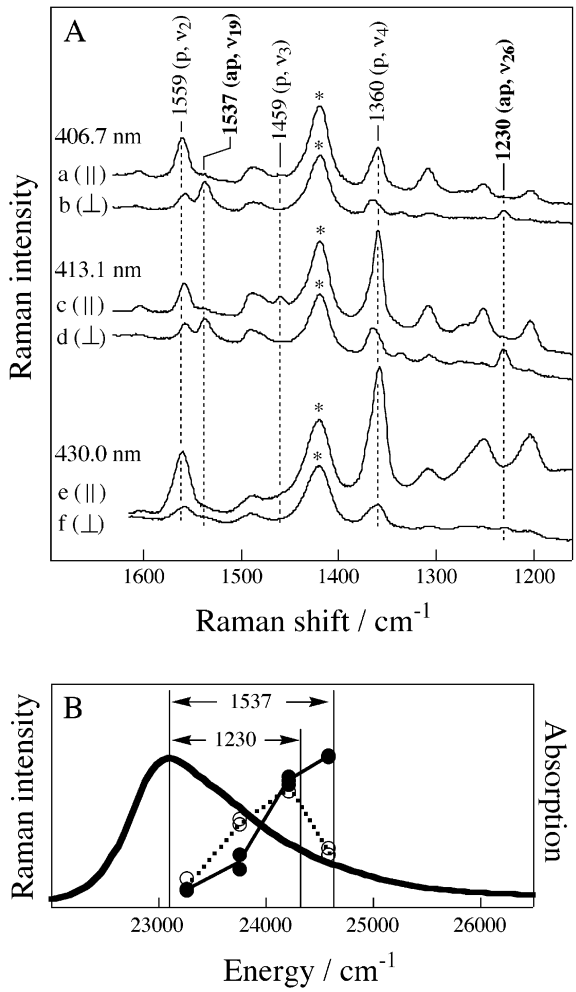

Figure 8. Resonance enhancements of A_{2g} Raman lines of iron(II) complex **2** upon excitation within the Soret band. (A) RR spectra of iron(II) complex **2** in DMSO upon excitation wavelengths at 406.7, 413.1, and 430.0 nm. The concentration of the sample was 33 μM. (B) REPs of the ν_{19} (closed circle) and ν_{26} (open circle) modes. The Soret band of iron(II) complex **2** is also illustrated on an arbitrary vertical scale.

the Soret and certain transition state(s), producing corresponding 0−1 vibronic sidebands.

Results essentially the same as those found for iron(II) complex 2 were also obtained with iron(II) complex **3**. Observed RR spectra and REPs of the ν_{19} and ν_{26} modes are shown in Figure 9, A and B, respectively.

Discussion

In this study, we could observe resonance enhancement of A_{2g} Raman lines for ferrous heme proteins and synthetic iron(II) porphyrin complexes upon excitation of Raman scattering within the Soret band. The dependency of band intensity on the excitation wavelength was satisfactorily correlated with these A_{2g} Raman lines; that is, these A_{2g} modes gained Raman intensity upon excitation at the 0−1 sideband of the Soret or red Soret transitions. Although Raman lines of the A_{2g} modes were also observed upon excitation at the 0−0 components, they were significantly weaker than those at the corresponding 0−1 sidebands. Because vibronic coupling between different electronic states is the sole source of Raman intensity for A_{2g} modes, the present findings indicate that the Soret or red Soret states of iron(II) porphyrins examined here hold vibronic coupling with other excited states.

Nonadiabatic Theories for the Vibronic Contribution to Raman Intensity. Theories for Raman scattering have described relationships between Raman intensity and electronic structures of molecules. Among them, the Albrecht theory, which employs adiabatic approximation for wave functions of vibronic states, must be the most well-known one.[39] Understanding observations of the Raman intensity of molecules including porphyrins, however, frequently needs a theoretical basis that is beyond the limit of the adiabatic approximation.[10,40−42] To achieve a general description for Raman intensity, which includes nonadiabatic vibronic coupling contributions, Shelnutt[10] derived a simple expression for vibronic terms of the scattering tensor within weak coupling limit as follows,[43]

$$B_{\rho\sigma}^{g1,g0}(a) = \sum_m \left[\frac{\sum_n M_\sigma^{gn} \frac{(H_a)_{nm}^0}{E_{m,0} - E_{n,1(a)}} M_\rho^{mg}}{E_{m,0} - E_{g,0} - h\nu - i\Gamma_{m,0}} + \frac{\sum_n M_\sigma^{gm} \frac{(H_a)_{nm}^0}{E_{m,1(a)} - E_{n,0}} M_\rho^{ng}}{E_{m,1(a)} - E_{g,0} - h\nu - i\Gamma_{m,1(a)}} \right] \quad (1)$$

where the suffix a stands for a normal coordinate mode Q_a, g and m are electronic wave functions in the crude Born−Oppenheimer treatment for the ground and mth excited states, n stands for all electronic excited states that affect the m state

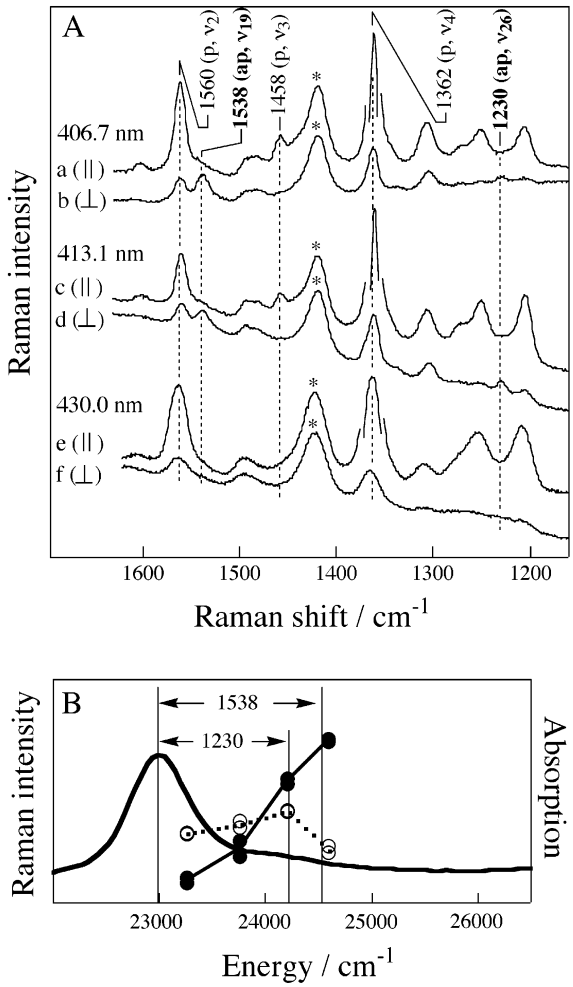

Figure 9. Resonance enhancements of A_{2g} Raman lines of iron(II) complex **3** upon excitation within the Soret band. (A) RR spectra of iron(II) complex **3** in DMSO upon excitation wavelengths at 406.7, 413.1, and 430.0 nm. The concentration of the sample was 33 μM. (B) REPs of the ν_{19} (closed circle) and ν_{26} (open circle) modes. The Soret band of iron(II) complex **3** is also illustrated on an arbitrary vertical scale.

through the vibronic coupling contributions, $M_{\sigma}^{gn} = \langle g|e\sigma|n\rangle$ and $M_{\rho}^{mg} = \langle m|e\rho|g\rangle$ etc., and $e\sigma$ and $e\rho$ are the σ- and ρ-th components of the electronic dipole operator, $E_{m,0}$, etc. are the energies of the vibronic states, $(H)^0_{anm}$ is the nm matrix element of the vibronic coupling operator for Q_a, ν is the frequency of the incident light for Raman scattering, and $\Gamma_{m,0}$ and $\Gamma_{m,1(a)}$ are bandwidths of the $|m\rangle|0\rangle$ and $|m\rangle|1(a)\rangle$ vibronic states.

When the frequency ν fully coincides with the 0−0 component of the m state and only n state has the vibronic interaction with the m state, the above equation can be reduced to

$$B_{\rho\sigma}^{g1,g0} = \frac{(-1/i\Gamma_m)\langle g|e\sigma|n\rangle\langle m|e\rho|g\rangle(H)^0_{nm}}{E_{m,0} - E_{n,1}} \qquad (2)$$

where the suffix a was omitted for simplicity and $\Gamma_{m,0}$ was simply denoted by Γ_m, on an assumption that $\Gamma_{m,0}$ and $\Gamma_{m,1}$ are essentially the same. Similarly, the excitation at the 0−1 component gives an expression for the scattering tensor as follows.

$$B_{\rho\sigma}^{g1,g0} = \frac{(-1/i\Gamma_m)\langle g|e\sigma|m\rangle\langle n|e\rho|g\rangle(H)^0_{nm}}{E_{m,1} - E_{n,0}} \qquad (3)$$

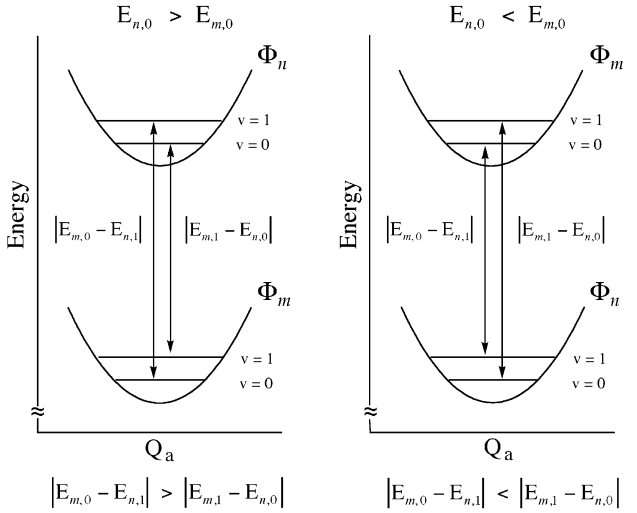

Figure 10. Schematic pictures for vibronic coupling between mth and nth electronic states.

Among the parameters in the above two equations, $\langle g|e\sigma|n\rangle\langle m|e\rho|g\rangle = -\langle g|e\sigma|m\rangle\langle n|e\rho|g\rangle$ when Q_a is an A_{2g} species of the D_{4h} symmetry.[10] Therefore, because the Raman intensity is proportional to the square of the scattering tensor, the Raman intensity ratio at the 0−0 to the 0−1 excitation for the A_{2g} species is predicted to be $[(E_{m,1} - E_{n,0})/(E_{m,0} - E_{n,1})]^2$. Similar conclusions have been also made by other groups, although mathematical formulas for expressing the scattering tensor are different over the groups.[40−42]

As illustrated in Figure 10, the sizes of $|E_{m,0} - E_{n,1}|$ and $|E_{m,1} - E_{n,0}|$ are asymmetric with respect to the relative energy levels of $E_{m,0}$ and $E_{n,0}$. If the mth electronic excited state vibronically couples with a higher energy excited state (left), $|E_{m,0} - E_{n,1}|$ is larger than $|E_{m,1} - E_{n,0}|$ by $2h\nu_a$ ($h\nu_a$, the vibration energy of the mode Q_a). In such a case, Raman intensity of mode Q_a must be smaller at m^{00} than at m^{01}. The intensity ratio is then given by $[(E_{n,0} - E_{m,0} - h\nu_a)/(E_{n,0} - E_{m,0} + h\nu_a)]^2$. This occurs when Raman scattering is excited within the porphyrin Q band, which holds vibronic coupling with the higher energy Soret band. Indeed, Raman lines of A_{2g} modes of porphyrins are more intense upon excitation at the β (=Q^{01}) band as compared to at the α (Q^{00}) band.[9,10] On the other hand, when mth electronic state couples with a lower energy excited state (Figure 10, right), the relation between $|E_{m,0} - E_{n,1}|$ and $|E_{m,1} - E_{n,0}|$ is reversed, making the band intensity excited at m^{00} larger than that at m^{01}. This is expected for Soret excited RR spectra if the vibronic coupling between the Soret and Q band states is the sole source of Raman intensity. On the basis of this, we analyzed the present results as described below, assuming that the weak coupling limit could apply

Origin of the Observed Vibronic Interactions. The present study showed that the A_{2g} Raman lines of the heme protein derivatives and the synthetic iron(II) complexes were more intense upon excitation at the 0−1 sidebands compared with that at the 0−0 band. These findings, together with the above discussions, indicate that the Soret (or red Soret) excited states of these derivatives and complexes hold significant vibronic interactions with certain higher energy excited state(s). To the observed REPs, vibronic interactions between B and Q band states must also contribute, but the contributions of the postulated higher energy state(s) overcome the former ones to produce the remarkably larger Raman intensity at the 0−1 band. This further indicates that the transition dipole of the higher

energy excited state(s) is significantly stronger than that of the Q band state.

The hyperporphyrins such as ferrous−CO and ferrous−isocyanide derivatives of $P450_{cam}$ exhibit the blue Soret band at higher energy neighborhood of their red Soret bands (Figure 2, inset, and Figure 5B). Therefore, it may be probable that the blue Soret states are the suggested higher energy states, which produce Raman intensity for ν_{19} mode via vibronic coupling with the red Soret states. Such an idea is, however, not likely, as discussed below.

As already described, the Raman intensity ratio in resonance with the m^{00} to m^{01} absorption band is given by $[(E_{n,0} - E_{m,0} - h\nu_a)/(E_{n,0} - E_{m,0} + h\nu_a)]^2$ when $E_{n,0}$ is larger than $E_{m,0}$. This relationship enables us to estimate the transition energy ($E_{n,0}$) of the higher energy excited state when values of $E_{m,0}$, ν_a, and the intensity ratio are given. For the present observation on ferrous−CO $P450_{cam}$, $E_{m,0}$ and ν_a in the above equation correspond to the transition energy of the red Soret band (22 422 cm^{-1}) and the frequency of ν_{19} (1584 cm^{-1}), respectively. Although the excitation wavelengths used here were not exactly coincident with the 0−0 and 0−1 components of the red Soret band of ferrous−CO $P450_{cam}$, the REP of ν_{19} (Figure 4D) enabled us to obtain an approximate value of the intensity ratio, and it was 0.63. On the basis of these experimental values, we estimated the transition energy of the higher energy excited state, which is involved in the vibronic interaction with the red Soret state, of ferrous−CO $P450_{cam}$ to be ~36 000 cm^{-1}. This energy value is significantly higher than the transition energy of the blue Soret band of ferrous−CO $P450_{cam}$ at 27 320 cm^{-1}. Accordingly, the red Soret excited state of ferrous−CO $P450_{cam}$, and possibly those of other hyperporphyrins examined, holds vibronic coupling with excited state(s) higher in energy than the blue Soret band.

Although REPs shown here are somewhat rough, it seems that the peaks in some of them are shifted slightly from the 0−1 absorption peaks toward 0−0 (e.g., Figures 4D and 5C). This shift can be explained in terms of the constructive interference effect (or filling-in effect), which is exclusively found for the A_{2g} modes among vibrations in D_{4h} compounds, being caused by phasing between vibronic contributions to Raman intensity at 0−0 and 0−1 transitions. [28]

Electronic Configuration of the Soret Excited States of Porphyrins. Shapes of optical absorption spectra of porphyrins in the Soret (or B) and Q band regions have been generally described on the basis of Gouterman's four-orbital model[1] which involves two HOMOs (a_{1u} and a_{2u}) and two LUMOs (e_{gx} and e_{gy}). The *x* and *y* components of the B^{00} and Q^{00} excited states are $B^{00}{}_x$, $[a_{2u}e_{gx}] - [a_{1u}e_{gy}]$; $B^{00}{}_y$, $[a_{2u}e_{gy}] + [a_{1u}e_{gx}]$, $Q^{00}{}_x$, $[a_{2u}e_{gx}] + [a_{1u}e_{gy}]$; $Q^{00}{}_y$, $[a_{2u}e_{gy}] - [a_{1u}e_{gx}]$. Because the Q^{01} band is produced by vibronic coupling between the B^{00} and Q^{00} electronic states, its *x* and *y* components can be represented as linear combinations of the above electronic configurations. Absorption bands assignable to the B^{01} transition are also frequently found in the optical spectra of porphyrins. The occurrence of the B^{01} band does not necessarily require vibronic coupling between different electronic states because the B^{01} transition as well as B^{00} is allowed. Therefore, the *x* and *y* components of the B^{01} state are essentially the same as those of B^{00}.

Being added to some extension, the four-orbital model has also explained the optical absorption spectra of hyperporphyrins.[1] A certain CT excited configuration having E_u symmetry takes part in the configuration interaction with the B^{00} state, inducing the splitting of the Soret band. Thus the blue and red Soret bands of hyperporphyrins share the same origin; the four-orbital configurations and CT electronic configurations that are differently weighted in the excited states of the two bands.

The present results indicate that the iron(II) normal- and hyperporphyrins examined here involve vibronic coupling between their Soret (or red Soret) states and some higher energy excited states. In other words, the Soret (or red Soret) states are mixed with the higher energy excited states. This finding indicates that the Soret (or red Soret) excited states of the present iron(II) porphyrins cannot be fully described as a combination of the four-orbital configurations and/or the CT configurations because porphyrin's excited sates to the blue of the Soret region employ other electronic configurations involving lower occupied orbitals.[44,45] If considering the excited configuration having E_u symmetry, which can hold vibronic coupling interaction with the Soret transition trough the A_{2g} modes, N and L band states employing $[b_{2u}\ e_g]$ and $[a'_{2u}\ e_g]$ configurations (a'_{2u}, the next-a_{2u}-HOMO), respectively,[44,45] must be the candidates for the higher energy states indicated here.

Involvement of contributions from the lower occupied orbitals in the Soret excited state has been suggested by SAC/SAC−CI quantum chemical calculations for free base porphyrin [46] and ferrous−CO hemoglobin.[3] On the other hand, experimental evidence employing RR techniques was reported for ferric myoglobin (metmyoglobin).[47] Using Kramers-Krönig transform techniques, Morikis et al. found the presence of a significant vibronic coupling contribution to Raman intensity for ν_3 Raman line of metmyoglobin upon Soret excitation.[47] Because such a contribution could not be attributed entirely to the vibronic coupling between the Soret and Q band states, they concluded the presence of vibronic coupling between Soret and higher energy electronic states.

Observing REPs of A_{2g} modes, we directly indicated the presence of vibronic coupling between the Soret and higher energy state(s) for iron(II) porphyrins for the first time. Involvement of contributions from lower occupied orbitals in the Soret states was demonstrated experimentally for the iron(II) porphyrins.

Acknowledgment. This work was supported in part by a Grant-in-Aid for scientific research on priority areas from Ministry of Education, Science, and Culture of the Japanese Government to H.S. and by the Joint Studies Program (2000−2001) of the Institute for Molecular Science to T.E. We are grateful to Dr. Takashi Yonetani (University of Pennsylvania, Philadelphia, PA) for critically reviewing the manuscript.

References and Notes

(1) Gouterman, M. *The Porphyrins*; Dolphin, D., Ed.; Academic Press: New York, 1978; Vol. 3; pp 1−165.
(2) Du, P.; Loew, G. H. *Biophys. J.* **1995**, *68*, 69−80, 4529.
(3) Tokita, Y.; Nakatsuji, H. *J. Phys. Chem. B* **1997**, *101*, 3281−3289.
(4) Hashimoto, T.; Choe, Y.-K.; Nakano, H.; Hirao, K. *J. Phys. Chem. A* **1999**, *103*, 1894−1904.
(5) Parusel, A. B. J.; Ghosh, A. *J. Phys. Chem. A* **2000**, *104*, 2504−2507.
(6) Spiro, T. G.; Strekas, T. C. *Proc. Natl. Acad. Sci. U.S.A.* **1972**, *69*, 2622−2626.
(7) Strekas, T. C.; Spiro, T. G. *Biochim. Biophys. Acta* **1972**, *278*, 188−192.
(8) Strekas, T. C.; Packer, A. J.; Spiro, T. G. *J. Raman Spectrosc.* **1973**, *1*, 197−206.
(9) Shelnutt, J. A.; Cheung, L. D.; Chang, C. C.; Yu, N.-T.; Felton, R. H. *J. Chem. Phys.* **1977**, *66*, 3387−3398.
(10) Shelnutt, J. A.; O'Shea, D. C. *J. Chem. Phys.* **1978**, *69*, 5361−5374.
(11) Cheung, L. D.; Yu, N.-T.; Felton, R. H. *Chem. Phys. Lett.* **1978**, *55*, 527−530.
(12) Parthasarathi, N.; Hansen, C.; Yamaguchi, S.; Spiro, T. G. *J. Am. Chem. Soc.* **1987**, *109*, 3865−3871.
(13) Shelnutt, J. A. *J. Chem. Phys.* **1981**, *74*, 6644−6657.

(14) Terner, J.; Topich, J. *Chem. Phys. Lett.* **1984**, *106*, 508−512.
(15) Teraoka, J.; Ishimaru, H. *Chem. Lett.* **1997**, *26*, 1293−1294.
(16) Imai, M.; Shimada, H.; Watanabe, Y.; Matsushima-Hibiya, Y.; Makino, R.; Koga, H.; Horiuchi, T.; Ishimura, Y. *Proc. Natl. Acad. Sci. U.S.A.* **1989**, *86*, 7823−7827.
(17) Egawa, T.; Shimada, H.; Ishimura, Y. *J. Biol. Chem.* **2000**, *275*, 34858−34866.
(18) Higuchi, T.; Uzu, S.; Hirobe, M. *J. Am. Chem. Soc.* **1990**, *112*, 7051−7053.
(19) Higuchi, T.; Shimada, K.; Maruyama, N.; Hirobe, M. *J. Am. Chem. Soc.* **1993**, *115*, 7551−7552.
(20) Suzuki, N.; Higuchi, T.; Urano, Y.; Kikuchi, K.; Uekusa, H.; Ohashi, Y.; Uchida, T.; Kitagawa, T.; Nagano, T. *J. Am. Chem. Soc.* **1999**, *11571−11572*.
(21) Dokoh, T.; Suzuki, N.; Higuchi, T.; Urano, Y.; Kikuchi, K.; Nagano, T. *J. Inorg. Biochem.* **2000**, *82*, 127−132.
(22) Hanson, L. K.; Eaton, W. A.; Sliger, S. G.; Gunsalus, I. C.; Gouterman, M.; Connell, C. R. *J. Am. Chem. Soc.* **1976**, *98*, 2672−2674.
(23) Loew, G. H.; Rohmer, M. M. *J. Am. Chem. Soc.* **1980**, *102*, 3655−3657.
(24) Dawson, J. H.; Andersson, L. A.; Sono, M. *J. Biol. Chem.* **1983**, *258*, 13637−13645.
(25) Jung, C. *Chem. Phys. Lett.* **1985**, *113*, 589−596.
(26) Miyahara, T.; Tokita, Y.; Nakatsuji, H. *J. Phys. Chem. B* **2001**, *105*, 7341−7352.
(27) Abe, M.; Kitagawa, T.; Kyogoku, Y. *J. Chem. Phys.* **1978**, *69*, 4526−4534.
(28) Felton, R. H.; Yu, N.-T. *The Porphyrins*; Dolphin, D., Ed.; Academic Press: New York, 1978; Vol. 3, pp 347−393.
(29) Kitagawa, T.; Abe, M.; Ogoshi, H. *J. Chem. Phys.* **1978**, *69*, 4516−4526.
(30) Spiro, T. G.; Strekas, T. C. *J. Am. Chem. Soc.* **1974**, *96*, 338−345.
(31) Ader, F.; Erecinska, M. *Arch. Biochem. Biophys.* **1974**, *165*, 570−580.
(32) Ader, F. *Arch. Biochem. Biophys.* **1975**, *170*, 644−650.
(33) Kitagawa, T.; Ozaki, Y. Struct. Bonding **1987**, *64*, 71−114.
(34) Unger, E.; Dreybrodt, W.; Schweitzer-Stenner, R. *J. Phys. Chem. A* **1997**, *101*, 5997−6007.
(35) Antonini, E., Brunori, M. *Hemoglobin and Myoglobin in Their Reactions with Ligands*; Neuberger, A., Tatum, E. L., Eds.; North-Holland Publishing Co: Amsterdam, 1971; Vol. 21, pp 13−39.
(36) Yu, C.-A.; Gunsalus, I. C.; Katagiri, M.; Suhara, K.; Takamori, S. *J. Biol. Chem.* **1974**, *249*, 94−101.
(37) Chang, C. K.; Dolphin, D. *J. Am. Chem. Soc.* **1975**, *97*, 5948−5950.
(38) Li, X.-Y.; Czernuszewicz, R. S.; Kincaid, J. R.; Su, Y. O.; Spiro, T. G. *J. Phys. Chem.* **1990**, *94*, 31−47.
(39) Tang, J., Albrecht, A. C. *Raman Spectroscopy − Theory and Practice*; Szymanski, H. A., Ed.; Plenum Press: New York, 1970; Vol. 2, pp 33−68.
(40) Zgierski, M. Z. *Chem. Phys. Lett.* **1975**, *36*, 390−392.
(41) Small, G. J.; Yeung, E. S. *Chem. Phys.* **1975**, *9*, 379−383.
(42) Johnson, B. B.; Nafie, L. A.; Peticolas, W. L. *Chem. Phys.* **1977**, *19*, 303−311.

(43) For the expression of eq 1, which is originally eq 13 of ref 10, some simplification might be done in the original study. In ref 10, Shelnutt employed a nonadiabatic expression for vibronic state as follows:

$$|m,\nu\rangle = |m_0\rangle|\nu\rangle + \sum_{\substack{n,u \\ (n,u\neq m,\nu)}} \frac{\langle u|\langle n_0|H_a Q_a|m_0\rangle|\nu\rangle}{E_{m,\nu} - E_{n,u}}|n_0\rangle|u\rangle$$

$$= |m_0\rangle|\nu\rangle + \sum_{\substack{n,u \\ (n,u\neq m,\nu)}} \frac{(H_a)^0_{nm}\langle u|Q_a|\nu\rangle}{E_{m,\nu} - E_{n,u}}|n_0\rangle|u\rangle \quad (4)$$

where $|u\rangle$ is vibrational wave function for the vibronic state $|n, u\rangle$ that takes part in vibronic coupling with the $|m,\nu\rangle$ state. The denominator of this expression, $E_{m,\nu} - E_{n,u}$, is the energy gap between the vibronic states, and it is distinct from corresponding denominator $E_{m,0} - E_{n,0}$ of the ordinary adiabatic expression used in the Albrecht's theory.[39] This difference results in a difference in the final expressions for Raman intensity. When eq 4 is used to obtain the expression for the scattering tensor in a manner similar to that employed in the Albrecht theory, a vibronic coupling term, which corresponds to the Albrecht B term, must be given for $|g,0\rangle \rightarrow |g,1\rangle$ Stokes Raman transition as follows:

$$B^{g1,g0}_{\rho\sigma}(a) = \sum_m \sum_n \sum_\nu \left[\frac{\langle 1|u\rangle\langle u|Q_a|\nu\rangle\langle\nu|0\rangle}{E_{m,\nu(a)} - E_{n,u(a)}} \frac{M^{gn}_\sigma (H_a)^0_{nm} M^{mg}_\rho}{E_{m,\nu(a)} - E_{g,0} - h\nu - i\Gamma_{m,\nu(a)}} + \frac{\langle 1|\nu\rangle\langle\nu|Q_a|u\rangle\langle u|0\rangle}{E_{m,\nu(a)} - E_{n,u(a)}} \frac{M^{gm}_\sigma (H_a)^0_{nm} M^{ng}_\rho}{E_{m,\nu(a)} - E_{g,0} - h\nu - i\Gamma_{m,\nu(a)}} \right] \quad (5)$$

This expression is similar to the Albrecht B term (the B term is indicated below)

$$B^{g1,g0}_{\rho\sigma}(a) = \sum_m \sum_n \sum_\nu \left[\frac{\langle 1|Q_a|\nu\rangle\langle\nu|0\rangle}{E_{m,0} - E_{n,0}} \frac{M^{gn}_\sigma (H_a)^0_{nm} M^{mg}_\rho}{E_{m,\nu(a)} - E_{g,0} - h\nu - i\Gamma_{m,\nu(a)}} + \frac{\langle 1|\nu\rangle\langle\nu|Q_a|0\rangle}{E_{m,0} - E_{n,0}} \frac{M^{gm}_\sigma (H_a)^0_{nm} M^{ng}_\rho}{E_{m,\nu(a)} - E_{g,0} - h\nu - i\Gamma_{m,\nu(a)}} \right] \quad (6)$$

but distinct from the B term in that the denominator of the first factor of each term is not $E_{m,0} - E_{n,0}$ but $E_{m,\nu} - E_{n,u}$, and the products of integrals of vibrational wave functions ($\langle 1|u\rangle\langle u|Q_a|\nu\rangle\langle\nu|0\rangle$, etc.) are those involving vibrational states of $|n,u\rangle$. The first term of eq 5 has a practical nonzero value when $\nu = 0$ and $u = 1$. This represents Raman scattering by vibronic coupling between $|m,0\rangle$ and $|n,1\rangle$ states. Similarly, the second term is nonzero when $\nu = 1$ and $u = 0$, representing vibronic coupling between $|m,1\rangle$ and $|n,0\rangle$ states. Therefore, eq 5 can be reduced to

$$B^{g1,g0}_{\rho\sigma}(a) = \sum_m \left[\frac{\sum_n M^{gn}_\sigma \frac{\langle 1|Q_a|0\rangle (H_a)^0_{nm}}{E_{m,0} - E_{n,1(a)}} M^{mg}_\rho}{E_{m,0} - E_{g,0} - h\nu - i\Gamma_{m,0}} + \frac{\sum_n M^{gm}_\sigma \frac{\langle 1|Q_a|0\rangle (H_a)^0_{nm}}{E_{m,1(a)} - E_{n,0}} M^{ng}_\rho}{E_{m,1(a)} - E_{g,0} - h\nu - i\Gamma_{m,1(a)}} \right] \quad (7)$$

If $\langle 1|Q_a|0\rangle$ in eq 7 is ignored, eq 7 can be reduced to eq 1. In the study of ref 10, Shelnutt might neglect this integral to obtain the final expression (i.e., eq 1 of this study, or eq 13 of ref 10) because this factor is not important in describing relative Raman intensity.

(44) Makinen, M. M.; Eaton, W. A. *Ann. N. Y. Acad. Sci.* **1973**, *206*, 210−222.
(45) Edwards, W. D.; Zerner, M. C. *Can. J. Chem.* **1985**, *63*, 1763−1772.
(46) Tokita, Y.; Hasegawa, J.; Nakatsuji, H. *J. Phys. Chem. A* **1998**, *102*, 1843−1849.
(47) Morikis, D.; Li, P.; Bangcharoenpaurpong, O.; Sage, J. T.; Champion, P. M. *J. Phys. Chem.* **1991**, *95*, 3391−3398.